Research Article

Residual Symmetries Applied to Neutrino Oscillations at NOνA and T2K

Andrew D. Hanlon,[1] Wayne W. Repko,[1] and Duane A. Dicus[2]

[1] *Department of Physics and Astronomy, Michigan State University, East Lansing, MI 48824, USA*
[2] *Department of Physics and Center for Particles and Fields, University of Texas, Austin, TX 78712, USA*

Correspondence should be addressed to Andrew D. Hanlon; adh58@pitt.edu

The results previously obtained from the model-independent application of a generalized hidden horizontal $\mathbb{Z}_2$ symmetry to the neutrino mass matrix are updated using the latest global fits for the neutrino oscillation parameters. The resulting prediction for the Dirac CP phase δ_D is in agreement with recent results from T2K. The distribution for the Jarlskog invariant J_ν has become sharper and appears to be approaching a particular region. The approximate effects of matter on long-baseline neutrino experiments are explored, and it is shown how the weak interactions between the neutrinos and the particles that make up the Earth can help to determine the mass hierarchy. A similar strategy is employed to show how NOνA and T2K could determine the octant of $\theta_a (\equiv \theta_{23})$. Finally, the exact effects of matter are obtained numerically in order to make comparisons with the form of the approximate solutions. From this analysis there emerge some interesting features of the effective mass eigenvalues.

1. Introduction

Although there has been significant progress in neutrino physics from oscillation experiments, there remains much work to be done. The reactor angle $\theta_r (\equiv \theta_{13})$ has now been measured to greater accuracy than ever before, and the solar angle $\theta_s (\equiv \theta_{12})$ has been known for some time now. But, the octant of the atmospheric angle ($\theta_a > \pi/2$ or $\theta_a < \pi/2$) or whether this angle is maximal ($\theta_a = \pi/2$) has yet to be answered. Determination of the Dirac CP phase has been improved. Recent results from T2K exclude at 90% C.L. $\delta_D \in [34.2°, 144°]$ for normal hierarchy (NH) and $\delta_D \in [-180°, -174.6°] \cup [-7.2°, 180°]$ for inverted hierarchy (IH) [1]. Finally, the absolute value of the mass squared differences has been carefully measured, but the mass hierarchy is still undetermined (i.e., $m_3 \gg m_2 > m_1$ or $m_2 > m_1 \gg m_3$). Each of these questions will be discussed in this work.

From the improvements in recent global analyses [2–4] it is possible to make more accurate predictions for the distributions of some of the aforementioned parameters of interest. Specifically, each of the residual symmetries, $\mathbb{Z}_2^s$ and $\overline{\mathbb{Z}}_2^s$, can be used to derive a model-independent equation for δ_D (one for each symmetry) [5, 6]. Then using the newly available global fits of the neutrino oscillation parameters in [2], likelihood distributions for δ_D, the Jarlskog invariant [7], and θ_a are obtained.

Using the PMNS mixing matrix, an expression for the probability of a neutrino originally of flavor α to be detected as a neutrino of flavor β, $P(\nu_\alpha \to \nu_\beta)$ is presented (which is a standard result found in many review papers on neutrino physics [8]). Then, using the approximation from [9] it is shown how the earth's matter affects the neutrino beam in long-baseline experiments. This is done by replacing the oscillation parameters with effective values that depend on the energy of the neutrinos, the baseline length, and the density of the matter.

In this paper, a focus is made on the NOνA and T2K experiments. Both of these experiments measure the appearance of ν_e's ($\bar{\nu}_e$'s) from a $\nu_\mu (\bar{\nu}_\mu)$ beam. The probability for this appearance is plotted as a function of energy using the best fits

TABLE 1: Global fits for neutrino oscillation parameters from [2]. * represents a local minimum at approximately 0.42σ for χ^2.

Parameter	Best fit	1σ range
$\sin^2\theta_s/10^{-1}$ (NH or IH)	3.08	2.91–3.25
$\sin^2\theta_r/10^{-2}$ (NH)	2.34	2.16–2.56
$\sin^2\theta_r/10^{-2}$ (IH)	2.39	2.18–2.60
$\sin^2\theta_a/10^{-1}$ (NH)	4.25	3.98–4.54
$\sin^2\theta_a/10^{-1}$ (IH)	4.37, 5.82*	4.08–4.96 ⊕ 5.31–6.10
δ_D/π (NH)	1.39	1.12–1.72
δ_D/π (IH)	1.35	0.96–1.59
$m_{21}^2/10^{-5}$ eV^2 (NH or IH)	7.54	7.32–7.80
$m_{31}^2/10^{-3}$ eV^2 (NH)	2.48	2.42–2.56
$|m_{31}^2|/10^{-3}$ eV^2 (IH)	2.36	2.29–2.43

for the oscillation parameters in [2]. The effects of matter are taken into account using the average matter density along the baseline for the two experiments. This is justified by the fact that there does not appear to be a significant effect due to the variation of the matter density [10]. A comparison is made for this probability with and without *CP*-violation in an attempt to observe the sensitivity of NOνA and T2K to measurements of δ_D. We have also plotted $P(\nu_\mu \to \nu_e)$ versus $P(\overline{\nu}_\mu \to \overline{\nu}_e)$ which shows that it may be possible for these experiments to determine the neutrino mass hierarchy for some values of the *CP* phase as discussed in [11, 12].

The update of the analysis of [13] given in [2] gives closer agreement on θ_a with the other two major global analyses [3, 4]. This shows that θ_a is closer to being maximal than originally believed and only excludes the possibility of it being maximal by about 1σ for inverted hierarchy. But, it is clear that the analyses do not agree upon which octant is favored. Fortunately, the plots of $P(\nu_\mu \to \nu_e)$ versus $P(\overline{\nu}_\mu \to \overline{\nu}_e)$ may also serve to determine the octant of θ_a [11, 12].

This work is concluded with a digression into the effective mixing angles and masses in matter. The solar resonance, first described by the MSW effect [14–16], and the atmospheric resonance are readily observed.

2. Distribution of δ_D, J_ν, and θ_a

The equations for δ_D, in terms of the neutrino mixing angles, based on residual symmetries are given by [5, 6]

$$\cos\delta_D = \frac{\left(s_s^2 - c_s^2 s_r^2\right)\left(s_a^2 - c_a^2\right)}{4c_a s_a c_s s_s s_r}, \tag{1a}$$

$$\cos\delta_D = \frac{\left(s_s^2 s_r^2 - c_s^2\right)\left(s_a^2 - c_a^2\right)}{4c_a s_a c_s s_s s_r}, \tag{1b}$$

for $\mathbb{Z}_2^s$ and $\overline{\mathbb{Z}}_2^s$ respectively, where $s_i \equiv \sin\theta_i$ and $c_i \equiv \cos\theta_i$. The latest global fits for the neutrino oscillation parameters from [2] are shown in Table 1.

From this we can obtain a distribution for $\cos\delta_D$ following the procedure in [5, 6] by using

$$\frac{dP\left(\cos\delta_D\right)}{d\cos\delta_D} = \int \delta_D^p \, \mathbb{P}\left(s_a^2\right)\mathbb{P}\left(s_s^2\right)\mathbb{P}\left(s_r^2\right)ds_a^2 ds_s^2 ds_r^2, \tag{2}$$

where $\delta_D^p \equiv \delta(\cos\delta_D - \overline{c}_D)$, the $\mathbb{P}$'s are proportional to $\exp(-\chi^2/2)$, and $\overline{c}_D \equiv$ RHS of (1a), (1b). Because it is preferable to get a distribution with respect to δ_D rather than $\cos\delta_D$ we use

$$\frac{dP\left(\delta_D\right)}{d\delta_D} = |s_D|\frac{dP\left(c_D\right)}{dc_D}, \tag{3}$$

where $c_D \equiv \cos\delta_D$ and $s_D \equiv \sin\delta_D$. Since this is a numerical integral, the delta function cannot be used as it is normally defined (unless integrated out of the equation prior to the numerical calculation). The integral was evaluated using a Monte Carlo algorithm and the results are shown in Figure 1(a). The domain of δ_D in (3) is $[-180°, 0°]$, but the distributions in Figure 1(a) can be reflected about $\delta_D = 0°$ to account for the full interval $[-180°, 180°]$. Therefore, these distributions have been normalized to $1/2$ over the domain shown in the figures. This means that each of the residual symmetries will have two peak predictions for the *CP* phase (equidistant from $0°$). The IH χ^2 curve for θ_a in [2] is closer to being symmetric about $\sin^2\theta_a = 0.5$. This is very prevalent in the results shown in Figure 1(a) given that the IH plots are close to being symmetric about $\delta_D = -90°$. But, since the NH global fit favors the lower octant for θ_a by at least 2σ [2] the predicted distributions for NH tend to prefer one side of $\delta_D = -90°$. But in both cases the results for $\mathbb{Z}_2^s$ are in agreement with the best fit value of $\delta_D = -90°$ from T2K's latest results [1].

The same method is applied to the Jarlskog invariant $J_\nu \equiv c_a s_a c_s s_s c_r^2 s_r s_D$ [7]; that is,

$$\frac{dP\left(J_\nu\right)}{dJ_\nu} = \int \delta_{J_\nu}^p \, \mathbb{P}\left(s_a^2\right)\mathbb{P}\left(s_s^2\right)\mathbb{P}\left(s_r^2\right)ds_a^2 ds_s^2 ds_r^2, \tag{4}$$

with $\delta_{J_\nu}^p \equiv \delta(J_\nu - c_a s_a c_s s_s c_r^2 s_r s_D)$. This distribution is shown in Figure 1(b). When calculating these distributions, δ_D is taken to be in the interval $[0, 180°]$ and is even about the vertical axis to extend δ_D to include $[-180°, 0°]$. To account for this, the figures are labeled for the distribution of $|J_\nu|$, and they can therefore be normalized to one. As compared with our previous results in [6], $\overline{\mathbb{Z}}_2^s$ is beginning to favor the region that $\mathbb{Z}_2^s$ prefers. Also, the region predicted by $\mathbb{Z}_2^s$ has become slightly narrower and it now excludes $|J_\nu| < 0.024$.

Finally, this method is again applied similarly to θ_a by first using (1a), (1b) to solve for $\tan 2\theta_a$

$$\tan 2\theta_a = \frac{c_s^2 s_r^2 - s_s^2}{2c_s s_s s_r \cos\delta_D}, \tag{5a}$$

$$\tan 2\theta_a = \frac{c_s^2 - s_s^2 s_r^2}{2c_s s_s s_r \cos\delta_D}, \tag{5b}$$
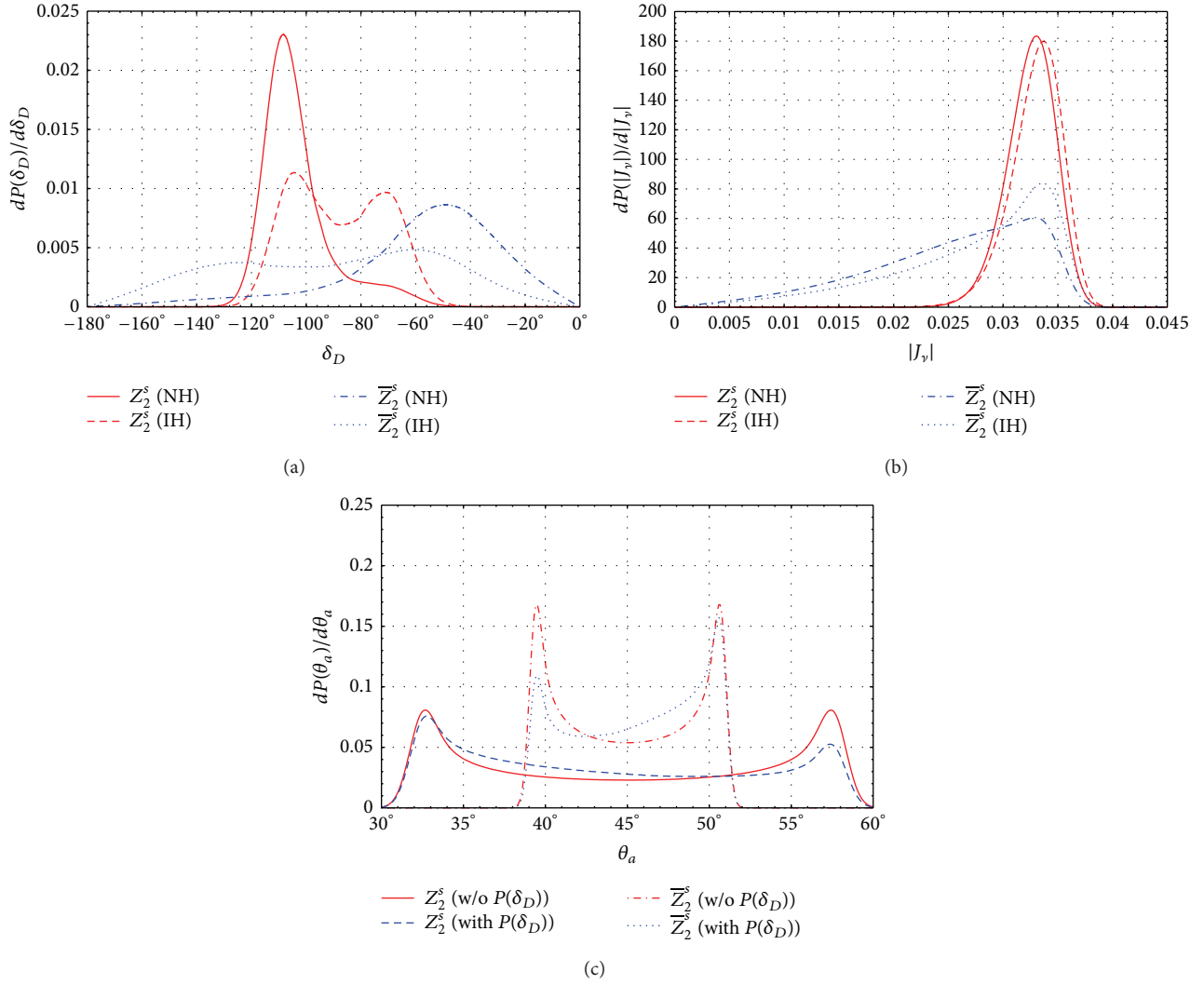
FIGURE 1: Predicted distributions for (a) δ_D, (b) J_ν, and (c) θ_a (NH) using the global analysis in [2].

for $\mathbb{Z}_2^s$ and $\overline{\mathbb{Z}}_2^s$, respectively. Then we have

$$\frac{dP\left(\tan 2\theta_a\right)}{d\tan 2\theta_a} = \int \delta_{\theta_a}^p \, \mathbb{P}\left(s_s^2\right) \mathbb{P}\left(s_r^2\right) \mathbb{P}\left(\delta_D\right) \mathrm{d}s_s^2 \mathrm{d}s_r^2 \mathrm{d}\delta_D, \quad (6)$$

with $\delta_{\theta_a}^p \equiv \delta(\tan 2\theta_a - \bar{t}_{\theta_a})$, where $\bar{t}_{\theta_a} \equiv$ RHS of (5a), (5b). To get a distribution for θ_a we use

$$\frac{dP\left(\theta_a\right)}{d\theta_a} = 2\sec^2\left(2\theta_a\right) \frac{dP\left(\tan 2\theta_a\right)}{d\tan 2\theta_a}. \quad (7)$$

The distribution is shown in Figure 1(c), where plots are made with and without using the prior on δ_D from [2]. When no prior on δ_D is used, $\mathbb{P}(\delta_D)$ becomes evenly distributed in $[0, 2\pi)$. As previously discussed in [6], θ_a is symmetric about $\theta_a = 45°$ when there is no prior on δ_D. In addition, the distributions using the prior on δ_D have also become more symmetric, as a result of the χ^2 for $\cos \delta_D$ also having become more symmetric about zero.

3. ν_μ to ν_e Oscillation

Now that we have a distribution for all the neutrino oscillation parameters, an attempt can be made to predict the results of an experiment measuring the number of ν_μ's that oscillate into ν_e's over some distance. First, the expression for this probability, $P(\nu_\mu \rightarrow \nu_e)$, must be found. Denoting the weak eigenstates of the neutrino by $|\nu_\alpha\rangle$ and the neutrino mass eigenstates by $|\nu_i\rangle$, then

$$\left(U_{\mathrm{PMNS}}\right)_{\alpha j} \equiv \left\langle \nu_\alpha \mid \nu_j \right\rangle \quad (8)$$

defines the PMNS mixing matrix, U_{PMNS}. The standard parametrization is given by [9]

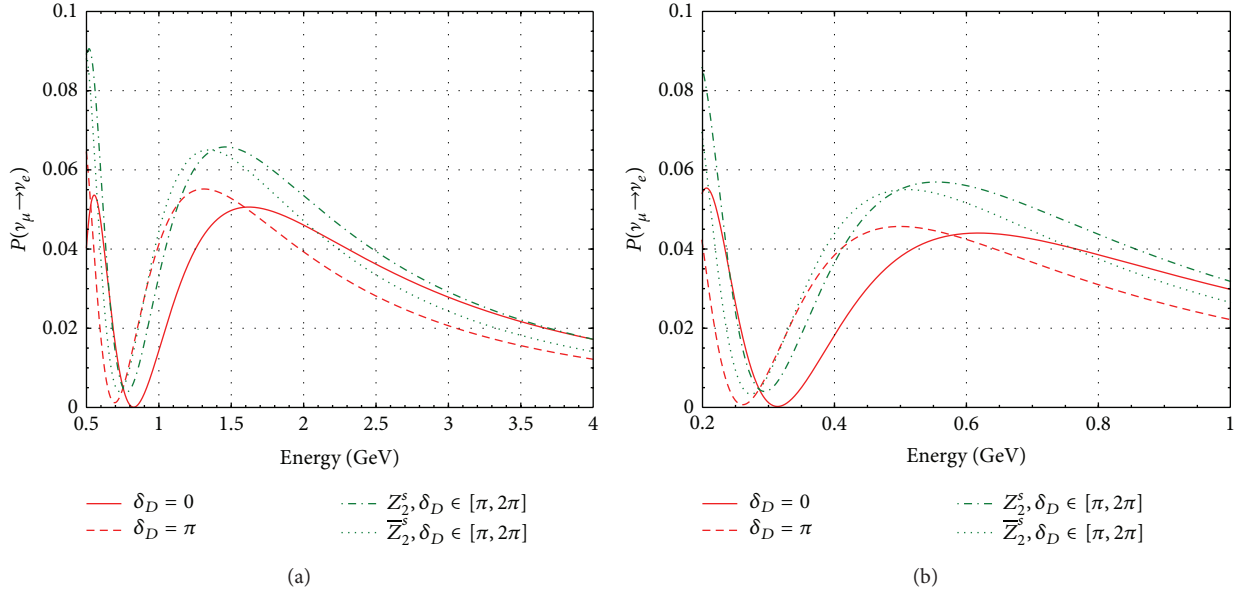$$U_{\mathrm{PMNS}} = U\mathscr{P}, \quad (9)$$

FIGURE 2: $P(\nu_\mu \rightarrow \nu_e)$ as a function of energy at (a) NOνA and (b) T2K, using the best fits from [2] with normal hierarchy.
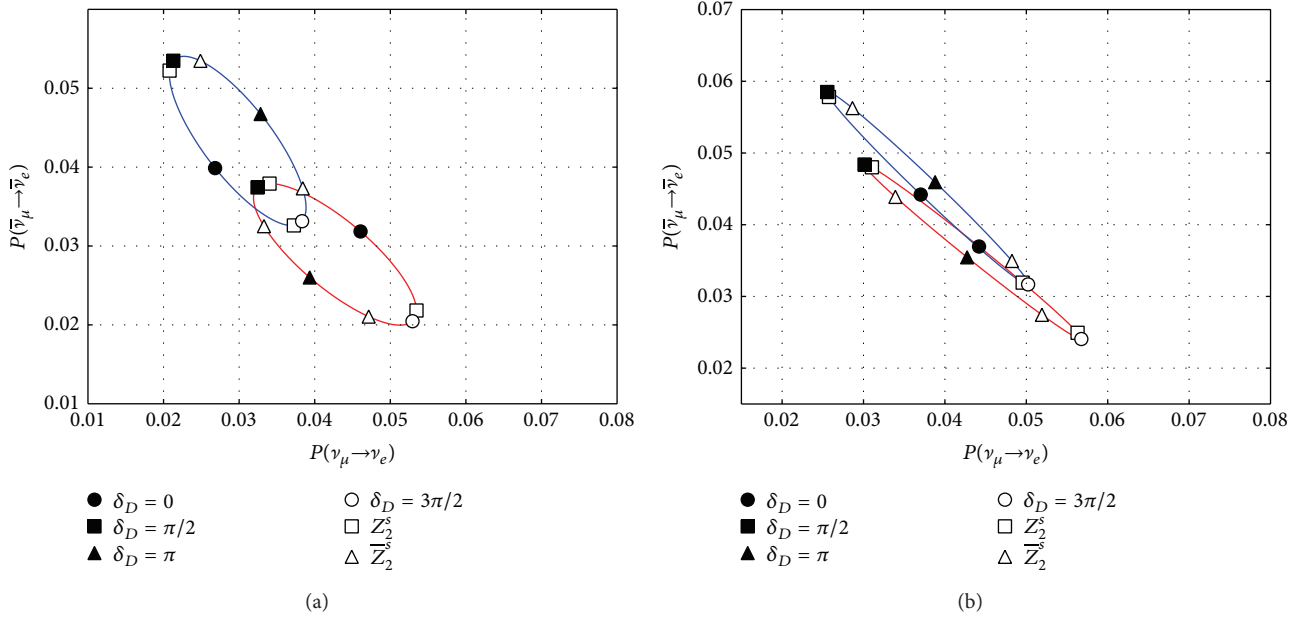

FIGURE 3: Plot of $P(\nu_\mu \rightarrow \nu_e)$ versus $P(\overline{\nu}_\mu \rightarrow \overline{\nu}_e)$ to show the sensitivity of (a) NOνA and (b) T2K to determine the mass hierarchy assuming $\theta_a < \pi/2$. The red ellipse (lower right corner) corresponds to NH, and the blue ellipse (upper left corner) corresponds to IH.

where

$$
U = \begin{pmatrix}
c_s c_r & s_s c_r & s_r e^{-i\delta_D} \\
-s_s c_a - c_s s_a s_r e^{i\delta_D} & c_s c_a - s_s s_a s_r e^{i\delta_D} & s_a c_r \\
s_s s_a - c_s c_a s_r e^{i\delta_D} & -c_s s_a - s_s c_a s_r e^{i\delta_D} & c_a c_r
\end{pmatrix}, \quad (10)
$$

$$
\mathscr{P} = \mathrm{diag}\left(1, e^{i\alpha_{21}/2}, e^{i\alpha_{31}/2}\right).
$$

From [8],

$$
\mathrm{Amp}\left(\nu_\alpha \longrightarrow \nu_\beta\right) = \sum_i U^*_{\alpha i} e^{-i m_i^2 (L/2E)} U_{\beta i}, \quad (11)
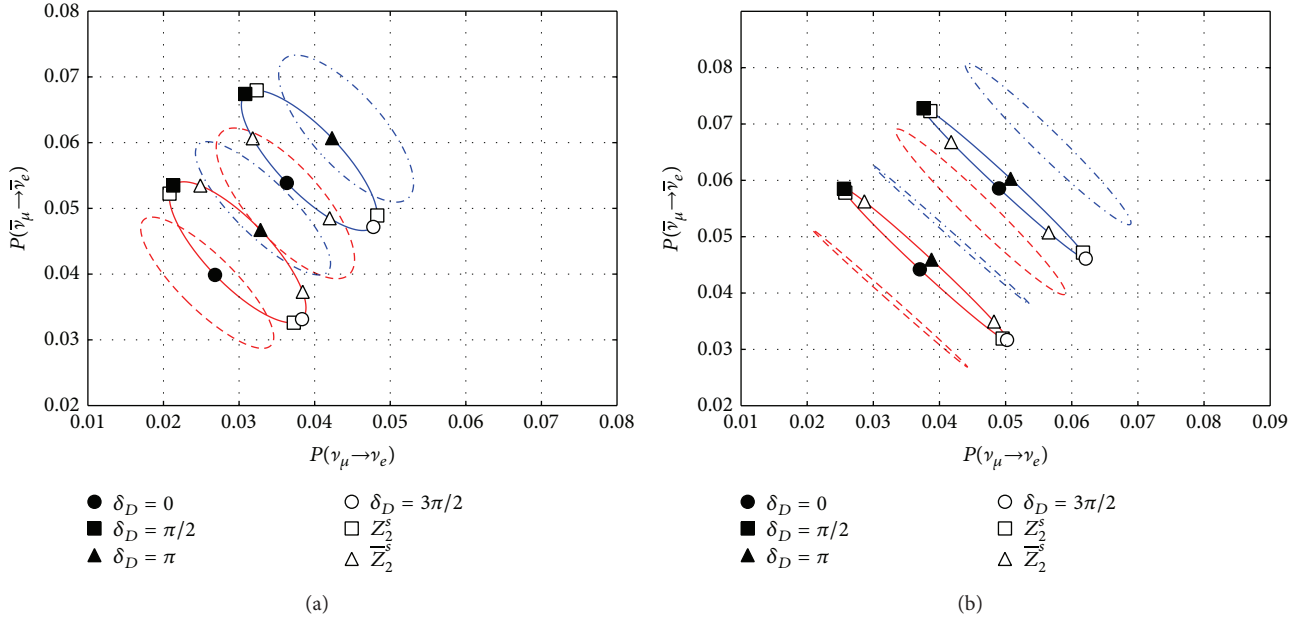$$

(a)

(b)

FIGURE 4: Plot of $P(\nu_\mu \rightarrow \nu_e)$ versus $P(\bar{\nu}_\mu \rightarrow \bar{\nu}_e)$ to show the sensitivity of (a) NOνA and (b) T2K to determine the octant of θ_a assuming inverted hierarchy. The red ellipses (lower left corner) correspond to $\theta_a < \pi/4$, while the blue ellipses (upper right corner) correspond to $\theta_a > \pi/4$. The dashed ellipses correspond to the $\pm 1\sigma$ values.

which leads to

$$P\left(\overset{(-)}{\nu_\alpha} \longrightarrow \overset{(-)}{\nu_\beta}\right)$$

$$= \delta_{\alpha\beta} - 4\sum_{i>j} \Re\left(U^*_{\alpha i} U_{\beta i} U_{\alpha j} U^*_{\beta j}\right) \sin^2\left(\Delta m^2_{ij} \frac{L}{4E}\right) \quad (12)$$

$$\overset{+}{(-)} 2\sum_{i>j} \Im\left(U^*_{\alpha i} U_{\beta i} U_{\alpha j} U^*_{\beta j}\right) \sin\left(\Delta m^2_{ij} \frac{L}{2E}\right),$$

where $\Delta m^2_{ij} \equiv m^2_i - m^2_j$, m_i is the ith mass eigenvalue, L is the distance propagated by the neutrino, and E is the energy of the neutrino. Notice that this probability does not depend on the Majorana phases, and therefore a discussion on these phases will not be pursued here.

Making the following definition [9]:

$$\Delta_{ij} \equiv \frac{\Delta m^2_{ij}}{2E} L \quad (13)$$

and noting that $\Delta_{32} = \Delta_{31} - \Delta_{21}$, then

$$P\left(\overset{(-)}{\nu_\mu} \longrightarrow \overset{(-)}{\nu_e}\right)$$

$$= 4s_s^2 c_r^2 \left(s_s^2 s_r^2 s_a^2 + c_s^2 c_a^2 - 2c_s c_a s_s s_r s_a c_D\right)$$

$$\times \sin^2\left(\frac{\Delta_{21}}{2}\right) + 4s_r^2 s_a^2 c_r^2 \sin^2\left(\frac{\Delta_{31}}{2}\right) + 2s_s s_r c_r^2 s_a$$

$$\times \left(c_s c_a c_D - s_s s_r s_a\right)$$

$$\times \left[4\sin^2\left(\frac{\Delta_{21}}{2}\right) \sin^2\left(\frac{\Delta_{31}}{2}\right) + \sin\left(\Delta_{21}\right) \sin\left(\Delta_{31}\right)\right]$$

$$\overset{+}{(-)} 4J_\nu \left[\sin^2\left(\frac{\Delta_{21}}{2}\right) \sin\left(\Delta_{31}\right)\right.$$

$$\left. -\sin^2\left(\frac{\Delta_{31}}{2}\right) \sin\left(\Delta_{21}\right)\right].$$

$$(14)$$

The last term includes the Jarlskog invariant [7] defined above.

3.1. Matter Effects.

As electron neutrinos propagate through the earth, they can interact with electrons via W-exchange. In addition, all three neutrino flavors can interact with electrons, protons, or neutrons via Z-exchange. Assuming electrically neutral matter, the Z-exchange between the neutrinos and protons will exactly cancel with the Z-exchange between the neutrinos and electrons [8]. The contribution from Z-exchange can be dropped, because it only adds a multiple of the identity matrix to the Hamiltonian [9]. Then, under the assumption that $E \ll M_W$, the effect of W-exchange can be accounted for by modifying the Hamiltonian for neutrinos [17]

$$H = \frac{1}{2E} U \begin{pmatrix} 0 & 0 & 0 \\ 0 & \Delta m^2_{21} & 0 \\ 0 & 0 & \Delta m^2_{31} \end{pmatrix} U^\dagger + \frac{1}{2E} \begin{pmatrix} a & 0 & 0 \\ 0 & 0 & 0 \\ 0 & 0 & 0 \end{pmatrix}, \quad (15)$$

where $a \equiv 2\sqrt{2}G_F N_e E$ and N_e is the density of electrons. For antineutrinos, the Hamiltonian is simply the complex conjugate of (15) with $a \rightarrow -a$.

One way to proceed is to diagonalize the Hamiltonian exactly, which has been done analytically [17–19]. However, this does not give much physical insight into the effects of matter on neutrino oscillations. Approximations in which the mixing angles and mass eigenvalues are replaced by effective values do not modify any of the equations, and therefore it becomes clear how matter affects neutrinos. A number of approximation schemes have been developed [20–26]. One of the most commonly used of these are the equations derived in [26]. But, due to the large value of θ_r measured at Daya Bay [27], the approximation in [26] begins to fail as is shown in [9]. In the approximation that is used here, the form of (14) can be used with the following modifications [9]:

$$\theta_s \longrightarrow \theta'_s, \qquad \theta_r \longrightarrow \theta'_r,$$
$$\Delta m^2_{21} \longrightarrow \lambda_2 - \lambda_1, \qquad \Delta m^2_{31} \longrightarrow \lambda_3 - \lambda_1, \tag{16}$$

with

$$\tan\left(2\theta'_s\right) = \frac{\left(\Delta m^2_{21}/c^2_r\right)\sin\left(2\theta_s\right)}{\left(\Delta m^2_{21}/c^2_r\right)\cos\left(2\theta_s\right) - a}, \tag{17a}$$

$$\tan\left(2\theta'_r\right) = \frac{\left(\Delta m^2_{31} - \Delta m^2_{21}s^2_s\right)\sin\left(2\theta_r\right)}{\left(\Delta m^2_{31} - \Delta m^2_{21}s^2_s\right)\cos\left(2\theta_r\right) - a}, \tag{17b}$$

$$\lambda'_{\pm} \equiv \left(\left(\Delta m^2_{21} + ac^2_r\right)\right.$$
$$\left. \pm \sqrt{\left(\Delta m^2_{21} - ac^2_r\right)^2 + 4ac^2_r s^2_s \Delta m^2_{21}}\right)(2)^{-1}, \tag{17c}$$

$$\lambda''_{\pm} \equiv \left(\lambda + \left(\Delta m^2_{31} + as^2_r\right)\right.$$
$$\left. \pm \sqrt{\left[\lambda - \left(\Delta m^2_{31} + as^2_r\right)\right]^2 + 4a^2 sc^2_r s^2_r}\right)(2)^{-1}, \tag{17d}$$

where for neutrinos let

$$\lambda \equiv \lambda'_+, \qquad s \equiv s'^2_s, \qquad \lambda_1 \approx \lambda'_-,$$
$$\lambda_2 \approx \lambda''_{\mp}, \qquad \lambda_3 \approx \lambda''_{\pm}, \tag{18}$$

and for antineutrinos let

$$\lambda \equiv \lambda'_-, \qquad s \equiv c'^2_s, \qquad a \longrightarrow -a,$$
$$\lambda_1 \approx \lambda''_{\mp}, \qquad \lambda_2 \approx \lambda'_+, \qquad \lambda_3 \approx \lambda''_{\pm}, \tag{19}$$

with the upper sign for normal hierarchy and the lower sign for inverted hierarchy.

It is helpful to show a and Δ_{ij} in conventional units. Following [9]

$$\Delta_{ij} = 2.534\left(\frac{\Delta m^2_{ij}}{[\text{eV}^2]}\right)\left(\frac{[\text{GeV}]}{E}\right)\left(\frac{L}{[\text{km}]}\right), \tag{20a}$$

$$a = \left(7.63 \times 10^{-5}\,[\text{eV}^2]\right)\left(\frac{\rho}{[\text{g/cm}^3]}\right)\left(\frac{E}{[\text{GeV}]}\right). \tag{20b}$$

3.2. NOνA and T2K. NOνA is a long-baseline neutrino oscillation experiment located in northern Minnesota. It has a baseline length of 810 km, an average matter density of 2.8 g/cm^3 along this baseline, and a peak neutrino energy around 2 GeV [11]. T2K is another neutrino oscillation experiment with similar goals to that of NOνA. Its baseline length is 295 km and has an average matter density of 2.6 g/cm^3, and the neutrino beam energy peaks around 0.6 GeV [28].

With the use of the effective mixing angles derived in the previous section, the probability of the appearance of a $\nu_e(\bar{\nu}_e)$ from a $\nu_\mu(\bar{\nu}_\mu)$ beam can be determined for any matter density. Using the length and matter density for the two experiments in question, plots of these probabilities are shown in Figure 2 as a function of energy.

It is not entirely apparent that the approximation [9] is valid for different values of the *CP* phase or the vacuum mixing angles; therefore, a comparison is made between this approximation and the exact results in the Appendix. In this comparison, the exact results are found by numerically diagonalizing the Hamiltonian. As it turns out, the approximation is very good for the energies and densities considered here.

4. Determination of the Mass Hierarchy and the Octant of θ_a

As has been mentioned previously, a major goal of neutrino oscillation experiments is to determine the mass hierarchy. If *CP* was a good symmetry, then there would be no observable difference between $P(\nu_\mu \rightarrow \nu_e)$ and $P(\bar{\nu}_\mu \rightarrow \bar{\nu}_e)$ when the neutrinos are propagating through a vacuum. However, interestingly enough, the matter effects discussed previously emulate the effects of *CP*-violation. Therefore, there is an observable difference between $P(\nu_\mu \rightarrow \nu_e)$ and $P(\bar{\nu}_\mu \rightarrow \bar{\nu}_e)$ even if *CP* is a good symmetry. Without the effects of matter the difference between oscillation probabilities for normal hierarchy versus inverted hierarchy is minimal. Thus it is because of the interactions with matter that allow for a discernible difference between normal and inverted hierarchy.

It is possible that actual *CP*-violation is substantially cancelled by this matter induced *CP*-violation. This would be very unfortunate, because it would make the determination of the *CP* phase more difficult than expected. A plot for $P(\nu_\mu \rightarrow \nu_e)$ versus $P(\bar{\nu}_\mu \rightarrow \bar{\nu}_e)$ is shown in Figure 3 for NOνA and T2K using the best fits from [2]. It can be seen that there are many values of the *CP* phase that will allow NOνA to make a serious determination of the true mass hierarchy. This will occur if $\delta_D \in [\pi, 2\pi]$ with NH being the true hierarchy or $\delta_D \in [0, \pi]$ with IH being the true hierarchy. And since T2K has excluded most of $\delta_D \in [0, \pi]$ at 90% C.L. [1], hopefully the true mass hierarchy is normal. From Figure 3(b) it appears that T2K will not be able to determine the mass hierarchy in this manner.

In addition, it may also be possible to determine the octant of θ_a from similar plots. These are shown in Figure 4. It appears that every value of the *CP* phase could at least give some indication of the true octant of θ_a, but the best values
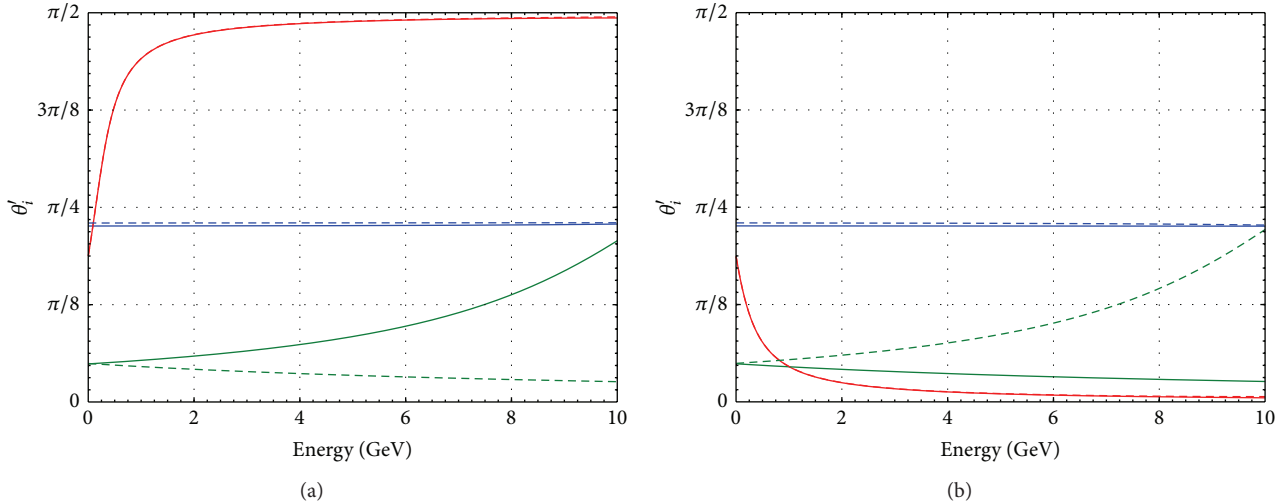
(a)												(b)

FIGURE 5: Plots of the effective mixing angles as a function of energy using data from [2]. For (a) NOνA and neutrinos, (b) NOνA and antineutrinos. Red = θ'_s, blue = θ'_a, and green = θ'_r. The solid lines are for normal hierarchy, and the dashed lines are for inverted hierarchy. In the cases where the dashed line is not visible, it's because the solid line is on top of it.

would be $\delta_D = 0$ for the lower octant and $\delta_D = \pi$ for the higher octant.

The ellipses were created by using (14) with the matter effect modifications of (16), for all possible values of δ_D (i.e., $\delta_D \in [0, 2\pi]$). The $\square$ and the $\triangle$ symbols correspond to the predicted values for δ_D, based on $\mathbb{Z}_2^s$ and $\overline{\mathbb{Z}}_2^s$, respectively. The predicted values are determined by using the best fits from [2] in (1a), (1b).

5. Effective Masses and Mixing Angles in Matter

The values of the effective mixing angles are plotted in Figure 5 and the mass eigenvalues in Figure 6, as functions of energy using the matter density for the NOνA experiment. The plots for T2K are excluded here, because they do not differ much from the ones for NOνA. Also, these particular plots consider $\delta_D = 0$, because the results depend very little on the CP phase. These have been plotted by numerically diagonalizing the Hamiltonian. It is assumed that the diagonalization matrix will have the same form as the standard parameterization of the PMNS mixing matrix.

The approximation introduced in Section 3.1 implies that the CP phase and θ'_a do not vary much, if at all, due to interactions with matter (which can be observed in Figure 5). It also implies certain characteristics of the variations of the other two mixing angles. From (17a), θ'_s should be independent of the mass hierarchy, and taking the limit $a \to \infty$, then $\theta'_s \to \pi/2 \, (0)$ for $\nu \, (\overline{\nu})$. This behavior is easily observed in Figure 5. From (17b), θ'_r should have similar asymptotic behavior as θ'_s for normal hierarchy, while it should reverse its behavior for inverted hierarchy. These features are approximately shown in Figure 5, but at the energies shown, θ'_r is not able to approach

its asymptotic limit. Therefore, these results appear to agree with the approximation in [9].

The effective neutrino masses are found from multiplying the eigenvalues of the Hamiltonian by $2E$. These plots are shown in Figure 6 for NOνA. There are some interesting characteristics of these plots. The first and most obvious are two resonances referred to as the solar resonance and the atmospheric resonance which represent the condition for maximal oscillation probability. This phenomenon was first understood with the introduction of the MSW effect [14, 15]. The first peak of $\sin^2(2\theta'_s)$ is the solar resonance and corresponds to an approach of $|\lambda_1|$ and $|\lambda_2|$ followed by a repulsion. The first peak of $\sin^2(2\theta'_r)$ is the atmospheric resonance and corresponds to an approach of $|\lambda_2|$ and $|\lambda_3|$ followed by a repulsion. If the absolute value of the mass eigenvalues crosses, then no resonance can be seen there. If we do not take the absolute value of the mass eigenvalues, then they will never cross each other. This is a wonderful example of level repulsion in quantum mechanics. For more details on these resonances, including a derivation of the resonance condition, see [14–16, 29].

6. Conclusions

Predicted distributions for δ_D, J_ν, and θ_a were updated using the residual symmetries $\mathbb{Z}_2^s$ and $\overline{\mathbb{Z}}_2^s$. It was found that the greater uncertainty in the octant of θ_a for IH shown in [2] forced the distributions of δ_D for IH to have nearly equal contributions on either side of $\delta_D = -90°$. This had no significant effect on the distribution for J_ν and the prediction for J_ν has improved.

By including the effects of matter into the oscillation probabilities, it was shown in Section 4 how NOνA stands a good chance of determining the mass hierarchy
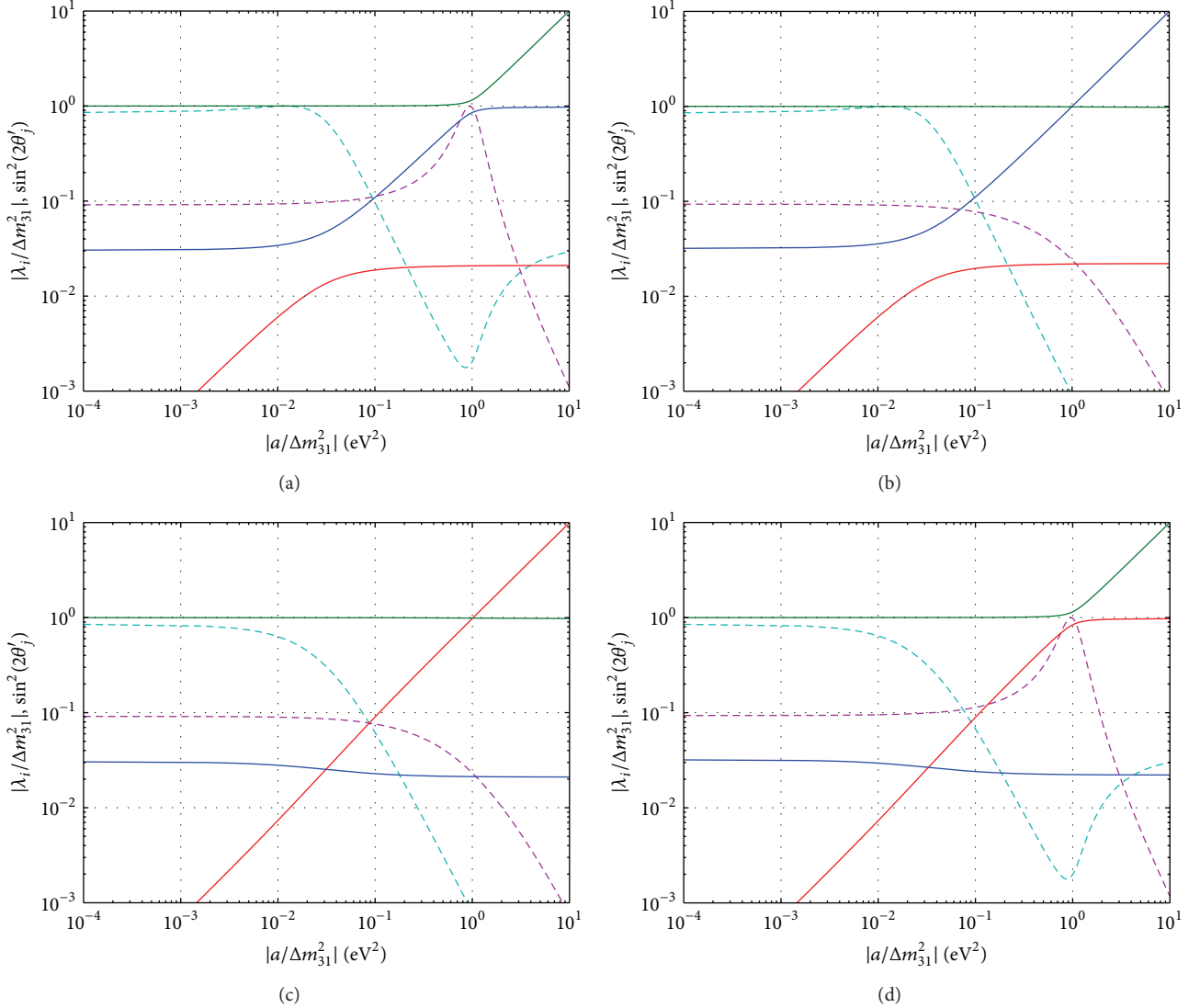
(a)

(b)

(c)

(d)

FIGURE 6: Effective masses for NOνA. The major focus of these plots should be on the solar and atmospheric resonances corresponding to a level repulsion. (a) ν and NH, (b) ν and IH, (c) $\bar{\nu}$ and NH, and (d) $\bar{\nu}$ and IH. Red = λ_1, blue = λ_2, green = λ_3, cyan-dashed = $\sin^2(2\theta_s)$, and magenta-dashed = $\sin^2(2\theta_r)$.

if $\delta_D \in [\pi, 2\pi]$ and the true hierarchy is normal or if $\delta_D \in [0, \pi]$ and the true hierarchy is inverted. It was also shown that both NOνA and T2K may be capable of nailing down the octant of θ_a.

The effects of matter were also shown to give rise to two resonances: the solar resonance and the atmospheric resonance. This behavior can be seen to agree with the approximation used throughout this work [9].

Appendix

Comparison with Solving for Matter Effects Exactly

Here a comparison is made between the approximation used [9] and exact results found from numerically diagonalizing

the Hamiltonian. Each plot for $P(\nu_\mu \to \nu_e)$ and $P(\bar{\nu}_\mu \to \bar{\nu}_e)$ above has been redone without any approximation. The plots in Figure 7 show the difference between these two methods. It is clear that the approximation is indeed very good, with a maximum difference around 0.0001.

Conflict of Interests

The authors declare that there is no conflict of interests regarding the publication of this paper.
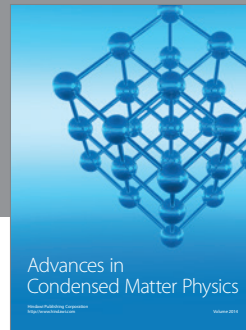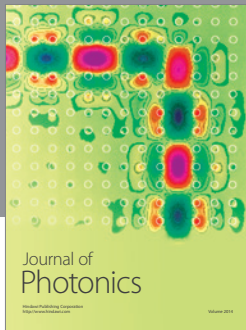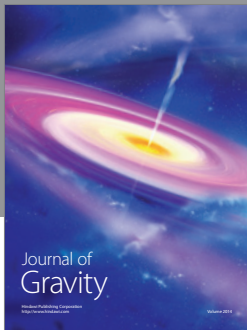
Acknowledgments
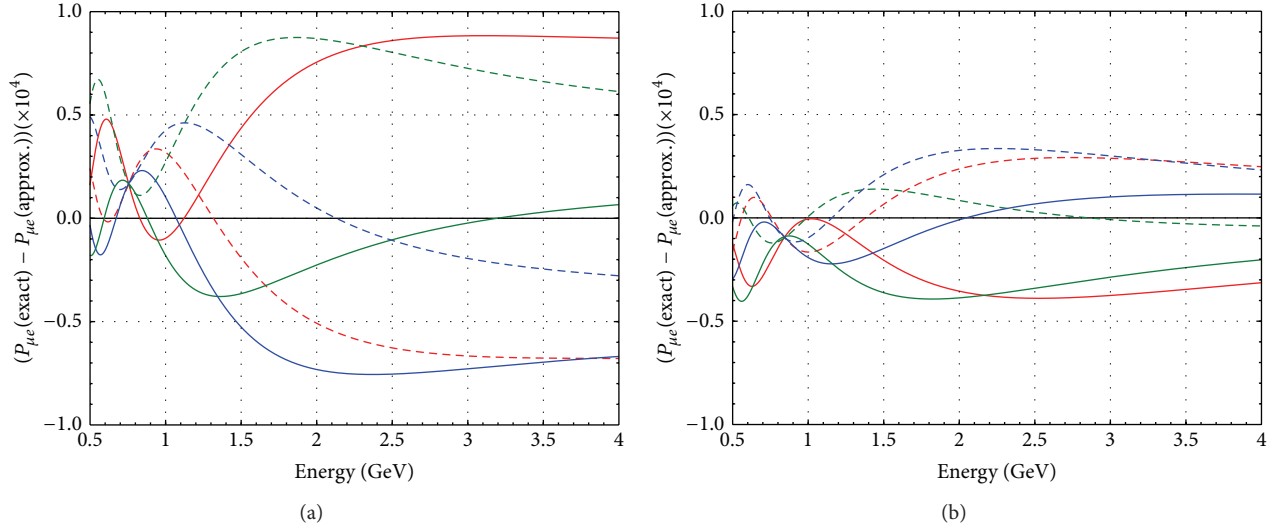
FIGURE 7: Comparison between the exact results and the approximation used throughout the paper. For (a) NOνA and neutrinos and (b) NOνA and antineutrinos. Red = ($\delta_D = 0$), red-dash = ($\delta_D = \pi$), green = $\mathbb{Z}_2^s$, $\delta_D \in [0, \pi]$, green-dash: = $\mathbb{Z}_2^s$, $\delta_D \in [\pi, 2\pi]$, blue: = $\overline{\mathbb{Z}}_2^s$, $\delta_D \in [0, \pi]$, and blue-dash: = $\overline{\mathbb{Z}}_2^s$, $\delta_D \in [\pi, 2\pi]$.

References

[1] K. Abe, J. Adam, H. Aihara et al., "Observation of electron neutrino appearance in a Muon neutrino beam," *Physical Review Letters*, vol. 112, Article ID 061802, 2014.

[2] F. Capozzi, G. Fogli, E. Lisi et al., "Status of three-neutrino oscillation parameters, circa 2013," *Physical Review D*, vol. 89, Article ID 093018, 2013.

[3] D. Forero, M. Tortola, and J. Valle, "Global status of neutrino oscillation parameters after Neutrino-2012," *Physical Review D*, vol. 86, Article ID 073012, 2012.

[4] M. Gonzalez-Garcia, M. Maltoni, J. Salvado, and T. Schwetz, "Global fit to three neutrino mixing: critical look at present precision," *Journal of High Energy Physics*, vol. 2012, article 123, 2012.

[5] S.-F. Ge, D. A. Dicus, and W. W. Repko, " Residual Symmetries for Neutrino Mixing with a Large theta_13 and Nearly Maximal delta_D," *Physical Review Letters*, vol. 108, Article ID 041801, 2012.

[6] A. D. Hanlon, S.-F. Ge, and W. W. Repko, "Phenomenological consequences of residual $\mathbb{Z}_2^s$ and $\mathbb{Z}_2^s$ symmetries," *Physics Letters B*, vol. 729, pp. 185–191, 2014.

[7] C. Jarlskog, "Commutator of the quark mass matrices in the standard electroweak model and a measure of maximal CP nonconservation," *Physical Review Letters*, vol. 55, p. 1039, 1985.

[8] B. Kayser, "Neutrino physics," eConf C040802, L004, http://arxiv.org/abs/hep-ph/0506165.

[9] S. K. Agarwalla, Y. Kao, and T. Takeuchi, "Analytical approximation of the neutrino oscillation probabilities at large θ_{13}," http://arxiv.org/abs/1302.6773.

[10] M. Koike and J. Sato, "Effects of matter density fluctuation in long baseline neutrino oscillation experiments," *Modern Physics Letters A*, vol. 14, no. 19, pp. 1297–1302, 1999.

[11] R. Patterson, "The NOνA experiment: status and outlook," *Nuclear Physics B—Proceedings Supplements*, vol. 235-236, pp. 151–157, 2013.

[12] S. K. Agarwalla, S. Prakash, and S. U. Sankar, "Resolving the octant of θ_{23} with T2K and NOνA," *Journal of High Energy Physics*, vol. 2013, article 131, 2013.

[13] G. L. Fogli, E. Lisi, A. Marrone, D. Montanino, A. Palazzo, and A. M. Rotunno, "Global analysis of neutrino masses, mixings and phases: entering the era of leptonic CP violation searches," *Physical Review D*, vol. 86, Article ID 013012, 2012.

[14] L. Wolfenstein, "Neutrino oscillations in matter," *Physical Review D*, vol. 17, pp. 2369–2374, 1978.

[15] S. Mikheev and A. Y. Smirnov, "Resonant amplification of ν oscillations in matter and solar-neutrino spectroscopy," *Il Nuovo Cimento C*, vol. 9, no. 1, pp. 17–26, 1986.

[16] A. Y. Smirnov, "The MSW effect and matter effects in neutrino oscillations," *Physica Scripta*, vol. 2005, no. T121, pp. 57–64, 2005.

[17] K. Kimura, A. Takamura, and H. Yokomakura, "Exact formulas and simple dependence of neutrino oscillation probabilities in matter with constant density," *Physical Review D*, vol. 66, Article ID 073005, p. 073005, 2002.

[18] H. W. Zaglauer and K. H. Schwarzer, "The mixing angles in matter for three generations of neutrinos and the MSW mechanism," *Zeitschrift für Physik C: Particles and Fields*, vol. 40, no. 2, pp. 273–282, 1988.

[19] K. Kimura, A. Takamura, and H. Yokomakura, "Exact formula of probability and CP violation for neutrino oscillations in matter," *Physics Letters B*, vol. 537, pp. 86–94, 2002.

[20] J. Arafune, M. Koike, and J. Sato, "CP violation and matter effect in long baseline neutrino oscillation experiments," *Physical Review D*, vol. 56, p. 3093, 1997.

[21] M. Freund, "Analytic approximations for three neutrino oscillation parameters and probabilities in matter," *Physical Review D*, vol. 64, Article ID 053003, 2001.

[22] O. Peres and A. Y. Smirnov, "Atmospheric neutrinos: LMA oscillations, U_{e3} induced interference and CP-violation," *Nuclear Physics B*, vol. 680, Article ID 0309312, pp. 479–509, 2004.

[23] E. K. Akhmedov, R. Johansson, M. Lindner, T. Ohls-son, and T. Schwetz, "Series expansions for three-flavor neutrino oscillation probabilities in matter," *Journal of High Energy Physics*, vol. 2004, article 078, 2004.

[24] E. K. Akhmedov, M. Tortola, and J. Valle, "A simple analytic three-flavour description of the day-night effect in the solar neutrino flux," *Journal of High Energy Physics*, vol. 2004, no. 5, article 057, 2004.

[25] E. K. Akhmedov and V. Niro, "An accurate analytic description of neutrino oscillations in matter," *Journal of High Energy Physics*, vol. 2008, no. 12, article 106, 2008.

[26] A. Cervera, A. Donini, M. Gavela et al., "Golden measurements at a neutrino factory," *Nuclear Physics B*, vol. 579, no. 1-2, pp. 17–55, 2000.

[27] D. A. Dwyer, "The improved measurement of electron-antineutrino disappearance at daya bay," http://arxiv.org/abs/1303.3863.

[28] K. Hagiwara, N. Okamura, and K.-I. Senda, "The earth matter effects in neutrino oscillation experiments from Tokai to Kamioka and Korea," *Journal of High Energy Physics*, vol. 82, 2011.

[29] J. Beringer, J.-F. Arguin, R. M. Barnett et al., "Review of particle physics," *Physical Review D*, vol. 86, no. 1, Article ID 010001, 2012.

[30] J. D. Hunter, "Matplotlib: a 2D graphics environment," *Computing in Science & Engineering*, vol. 9, pp. 90–95, 2007.